doi:10.1038/nature10684

1 PLANET microlensing data 2002-2007

1.1 PLANET observing strategy 2002-2007

Since the discovery of the first extrasolar planet orbiting a main-sequence star[31], the search for new worlds outside of our Solar System has undergone significant progress, counting now more than 600 exoplanets. While most of those planets are massive gas giants, already a few telluric exoplanets with masses of only a few times that of the Earth have been found.

The technique of gravitational microlensing is ideally suited to obtain a sample of planets below ten Earth masses at several astronomical units from their parent stars (0.5-10 AU), a region of planet parameter space that is hardly accessible by other technique. The planets found by microlensing are preferentially orbiting stars located at 1-8 kpc, *i.e.* far beyond the Solar neighbourhood and thus affording an unmatched probe of the population of extrasolar planets across the Galaxy. Moreover, the technique has very little bias on host star masses. Microlensing is thus mainly probing planetary systems around the most common stars of the Galaxy (M-K dwarfs), but solar or more massive host stars are also part of the sample.

Survey teams like OGLE[a,(32)] and MOA[b,(33)] have reported more than six thousand microlensing events toward the Galactic bulge to date. Many hundreds of these events have been carefully selected and densely sampled by follow-up networks such as PLANET[c], μFUN[d], RoboNet[e] and MiNDSTEp[f]. Since its pilot season in 1995, the PLANET (Probing Lensing Anomalies NETwork) collaboration[34] has been active in monitoring Galactic microlensing events, with the ambition to obtain a microlensing census of planets around all stars over the full mass range from massive gas giants to terrestrial planets.

Originally[35], the main reason for establishing follow-up collaborations was based on the fact that the observing cadence of a large microlensing survey was too low and therefore not sufficient to unambiguously establish the planetary nature of a light curve deviation. Hence, running survey observations alone would severely restrict establishing reliable planet abundance statistics, especially related to low-mass planets. To address this problem, Ref. (35) pressed for a strategy of intense monitoring of a sub-sample of events chosen from microlensing alerts

[a] http://www.astrouw.edu.pl/~ogle
[b] http://www.phys.canterbury.ac.nz/moa
[c] http://planet.iap.fr
[d] http://www.astronomy.ohio-state.edu/~microfun
[e] http://robonet.lcogt.net
[f] http://www.mindstep-science.org

issued by survey group, in particular OGLE.

In 2002-2007, the observing strategy adopted by PLANET consisted of following up a selection of OGLE III events with high cadence and round-the-clock sampling with a global network of telescopes. The sampling rate was increased with the magnification rising towards the peak of the light curve, or in response to the real-time anomaly alerts (including alerts from OGLE). Since PLANET applied the same selection criteria and follow-up rules regardless of whether the lens harbours a planet or not, the sample can be regarded as homogeneous both for detections and non-detections, provided that planetary anomalies can be detected with the adopted strategy. In fact, Ref. (36) already based their estimation of upper limits on planet abundance on such homogeneous samples, although the strategy adopted for the range of time considered (1995-2000) was different.

1.2 Microlensing non-planetary events selection

While microlensing survey light curves alone already provide a significant detection efficiency to giant planets[37], statistics from low-mass planets can only arise from events that are more densely sampled (since short-lived planetary signals can more easily fit in gaps of the data coverage). The ensemble of events we use in the present study has much more sensitivity than these previous studies, especially for low-mass planets. In fact, our sample includes many more very well-covered events with a range of peak magnifications, which thus probe more efficiently the parameter space where planet signals reside.

Following Ref. (38), we use the non-detections to compute the detection efficiency of PLANET 2002-2007 observations. In order to draw meaningful statistical results, it is crucial that the observing strategy stays homogeneous for the time span considered in the analysis. When starting its new operations in 2002, OGLE III dramatically increased its number of issued alerts (389 alerts in 2002 compared to 78 alerts in 2000 with OGLE II), which had a strong impact on the PLANET strategy. From 2002 to 2007, PLANET then operated with the same consistent strategy, but after that, was much more influenced by other teams, in particular for very high-magnification events. For consistency, we then limit ourselves to extending the analysis to seasons 2002-2007 (see also Fig. S2 and related discussion).

The OGLE Collaboration respectively alerted 389, 462, 608, 597, 581 and 610 events for 2002-2007, from which PLANET monitored (with a range of data quality and sampling) 40, 51, 98, 83, 96 and 72 light curves. The ratio between the events monitored by PLANET and

OGLE alerts ranges from $\sim 10-16\%$ with a mean around 13%.

We choose 2004 as a typical season of the PLANET follow-up strategy in 2002-2007. Since the precision of the detection efficiency calculation depends on the quality of the data (Section 2), not all light curves can be processed. We therefore adopt the same light curve selection criteria as Ref. (36) (*i.e.*, no clear light curve deviation from a single lens, more than 20 PLANET data, $\delta u_0/u_0 \leq 50\,\%$), and same data reduction (based on DoPhot[39]) and cleaning procedures to build a catalogue of suitable events.

Amongst the 98 events monitored in 2004, we extract 43 light curves, from which 26 provide stable and robust detection efficiency measurements for the chosen ranges of planet orbits and masses. Moreover, this selection still is a representative sample of OGLE alerts, since the event selection procedure is based on the data quality and not on the characteristics of the events themselves (like their peak magnifications). In Table S1, we list the selected microlensing events with their characteristics and the quality criteria they passed.

2 Microlensing planet detection efficiency

2.1 Basics of microlensing light curve modelling

If the angular separation between a source background star located at distance D_S and a foreground object with mass M located at D_L happens to be of order of the angular Einstein ring radius[40]

$$\theta_E = \sqrt{\frac{4GM}{c^2}\left(\frac{D_S - D_L}{D_S D_L}\right)}, \tag{1}$$

a "microlensing effect" occurs and the source is substantially magnified[41].

Most microlensing light curves are well-explained by point-source single-lens models, which involve three model parameters: t_E, the time for the source to travel θ_E; u_0, the minimum impact parameter between lens and source expressed in θ_E units, and t_0, the time at u_0. Nevertheless, as pointed out by Refs. (42) and (35), a planet around the lens can reveal its presence by distorting the observed single-lens light curve. In the framework adopted in this study, planets are modelled as binary lenses, that introduce three additional model parameters: the planet-star mass ratio q and its separation d in θ_E units and α, the angle of the source trajectory relative to the star-planet axis.

Fitting a magnification model $A(t)$ to the observational data requires computing two more

parameters per distinct data set n (different telescope or filter). In fact, the observed flux can be expressed as the sum of a blending flux ${F_B}^n$ that includes the light contribution from the lens and other unrelated background stars, and the source flux ${F_S}^n$ magnified due to the lens by a factor $A(t)$, so that the total flux reads

$$F^n(t) = A(t)\,{F_S}^n + {F_B}^n \tag{2}$$

for each individual data set n.

2.2 Detection sensitivity 2002-2007

The planet detection efficiency $\varepsilon(\log d, \log q)$ is the probability that a detectable planet signal would arise if the lens star has a companion with mass ratio q and separation d. In practice, we choose to use $\log q$ and $\log d$ because the detection efficiency then displays a naturally symmetric behaviour. Following Ref. (38), we refer to a planet signal as the χ^2-excess introduced by a binary-lens model ("BL") with (d, q), relative to the best single-lens model ("SL") fitting the data, *i.e.* $\Delta\chi^2 = \chi^2_{\rm BL} - \chi^2_{\rm SL}$. A detectable signal is then defined by $\Delta\chi^2$ exceeding a fixed threshold value χ_t. As Ref. (36) pointed out, Monte-Carlo simulations based on PLANET photometry of constant stars has shown that a $\chi_t = 60$ can account for false detections arising from statistical fluctuations or low-level systematics. However, as argued in Ref. (43), this threshold is usually too low to characterise planets detected upon signals just above the statistical fluctuation level. For typical light curves of our sampling – regular but not extremely aggressive sampling, relatively low-magnification events – a threshold of $\chi_t = 300$ is a conservative choice, that would allow the detection of a planet like OGLE 2005-BLG-390Lb. Planets like MOA 2007-BLG-400Lb would require a higher threshold, but in this particular case, the planet was detected with a very different strategy.

To compute the detection efficiency $\varepsilon(\log d, \log q)$ for a chosen grid of binary lenses in the plane $(\log d, \log q)$, we use the algorithm described in Ref. (38): for a given microlensing light curve that does not show evidence of anomaly, we fit a single-lens model to the data and rescale the error bars so that $\chi^2/\text{d.o.f.}_k = 1$ for every individual data set (a σ-clipping procedure is applied to compute the rescaling factors, but all data are included again afterwards). The computation of $\varepsilon(\log d, \log q)$ then amounts to determining the fraction of the source trajectory angles $0 \leq \alpha \leq 2\pi$ for which $\Delta\chi^2(d, q, \alpha) > \chi_t$. We choose 400 steps in α, which corresponds to a precision of $\delta\varepsilon = 0.25\%$ in the calculation.

Our software package TANGOBI[44; 45; 46; 47] designed for detection efficiency calculations uses a grid of 230 pre-computed magnification maps[48], which speeds up the computations (a critical aspect here) and allows a robust treatment of finite source effects. The (logarithmically spaced) grid covers the ranges $0.1 \leq d \leq 10$ and $10^{-5} \leq q \leq 10^{-2}$, with a denser sampling in the "lensing zone" ($0.6 \leq d \leq 1.6$).

We account for finite-source effects in the modelling by introducing an additional parameter ρ_*, the source's angular radius in $\theta_{\rm E}$ units. To derive its value, we first need to estimate the physical radii of the source stars. By drawing a histogram of the full OGLE light curves source magnitudes from seasons 2002-2007, we clearly distinguish a peak for the Main Sequence and a peak for giant stars, with a transition magnitude at $I_0 \simeq 17$. Each individual microlensing event is then assigned a type based on its OGLE best-fit source magnitude, either "giant" with $R_* = 10\,R_\odot$ or "main sequence" with $R_* = R_\odot$. When 2MASS data were available (for a couple of events only), we have checked that the source radii were correctly estimated. We then combine the information on $t_{\rm E}$ and R_* using again the model of Ref. (49) to derive an estimation of ρ_*. We find that for the sample of events used in this work, the three grid values 10^{-3}, 2.5×10^{-2} and 10^{-2} for ρ_* provide sufficient accuracy for sampling the sizes of the source stars. The magnification maps for each of the three source sizes are then convolved with a linear limb-darkened source (of fixed coefficient $a_{\rm LLD} = 0.5$). After fitting, the final $\varepsilon(\log d, \log q)$ for a given event is then determined by interpolating between the source size grid.

Planet observations or formation theories are usually expressed in terms of the planetary mass M and orbital semi-major axis a. To convert our efficiency $\varepsilon(\log d, \log q)$ into these parameters, we adopt the Bayesian approach based on the measured value of $t_{\rm E}$ and detailed in Ref. (49), which leads to $\varepsilon(\log r, \log M)$, where r refers to the projected planet-star separation in AU. In a further step, the desired efficiency $\varepsilon \equiv \varepsilon(\log a, \log M)$ is obtained by convolving $\varepsilon(\log r, \log M)$ over r assuming isotropic circular orbits for the planets[50].

We define the planet detection sensitivity $S(\log a, \log M)$ as the expected number of planets that our survey can detect if all lens stars have exactly one planet of mass M and orbit size a, which reads

$$S(\log a, \log M) \equiv \sum_{n=1}^{N} \varepsilon(n)\,, \tag{3}$$

where N is the total number of events included in the analysis.

For the reference season 2004, we find that the detection efficiency is well described by a power law $\varepsilon(n) \simeq \varepsilon_0 \times 10^{-\gamma n}$, with n the events ordered by decreasing detection efficiency, and

$\gamma > 0$. We find a similar behaviour for seven of the best events in season 2003 (Table S1). It means that in practice, we observe an equal number of events per decade of detection efficiency, from which it follows that only a fraction of all followed-up events significantly contribute to the analysis. For example, out of the 43 events that were monitored densely by PLANET from 1995-1999, Ref. (36) found that only 8 light curves accounted practically for all of the detection efficiency.

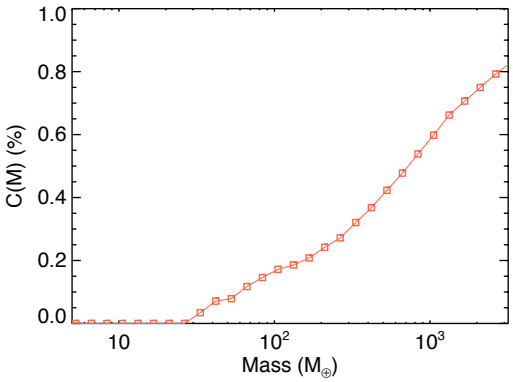

Figure S1: Relative contribution (in %) of the least contributing event included in the 2004 event sample, integrated over $\log a$ and as a function of planet mass M. Its maximal contribution is reached at 10 $M_{\rm J}$, with $C(M) \leq 0.85\%$.

In order to further estimate how many events should then be included in the analysis, we compute for season 2004 the relative contribution of the least contributing event (*i.e.* the last event, indexed N), integrated over $\log a$ and as a function of mass

$$C(M) = \frac{\int \varepsilon(N)\, \mathrm{d}\log a}{\sum_{n=1}^{N} \int \varepsilon(n)\, \mathrm{d}\log a}\,. \tag{4}$$

The resulting function $C(M)$ is plotted in Fig. S1. It shows that the least contributing event included has a contribution that grows with mass up to 0.85% (reached at $10 M_{\rm J}$). Since our PLANET non-detection sample contains most of the contributing events, we can therefore regard the selection of the 2004 season events as a fair representation of the PLANET detection sensitivity, with a relative error smaller than 1%.

As already mentioned, during 2002-2007 PLANET operated with a very similar observing

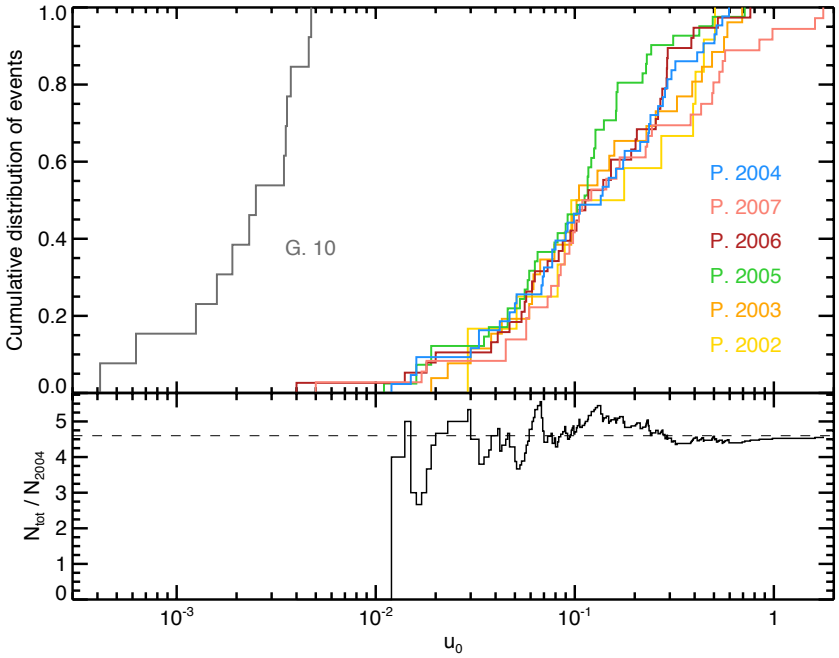

Figure S2: Upper panel: Cumulative distributions of the impact parameter u_0 for the events that passed our selection criteria, each of the 2002-2007 seasons (coloured curves, labelled "P. 200x"). The events are given in Table S1. For comparison, the cumulative distribution for high-magnification events (labelled "G. 10") included in the analysis of Ref. (43) is also shown (see the text for the discussion of this figure). Lower panel: The solid curve shows the ratio between the cumulative distribution of u_0 for all events in 2002-2007, and the cumulative distribution for 2004 alone. The dashed line indicates the equivalent number of seasons when using 2004 as a reference season.

strategy, choosing events alerted by OGLE, and following up a subset of them. In order to estimate precisely how the reference season 2004 compares to other seasons, we have extracted from the full set of PLANET events all light curves that passed the selection criteria recalled in Section 1.2. We obtain 12 light curves for 2002, 26 for 2003, 43 for 2004 (as mentioned before), 41 for 2005, 38 for 2006, and 36 for 2007. The corresponding list of events is given in Table S1. The cumulative distributions of the impact parameter u_0 (i.e., by inverse order of their peak magnification) is plotted on the upper panel of Fig. S2 for each season (labelled "P. 200x"). The cumulative histograms clearly have a very similar behaviour, thus supporting that the observing strategy was very homogeneous in this time span. For comparison, we have plotted in grey (and labelled "G. 10") the cumulative distribution of u_0 for the set of high-magnification events included in the analysis of Ref. (43). The plot itself demonstrates that the selection of events and observing strategy was very different and not comparable with PLANET strategy.

A consequence of the similar distributions of peak magnifications amongst the seasons is that the sensitivity in the time span 2002-2007 can be fairly approximated by a correction factor on the number of events. In the lower panel of Fig. S2, we have plotted the ratio of the cumulative distribution of the total number of events and the cumulative distribution of the number of events in 2004, as a function of u_0. We find that a correction factor of $\kappa = 4.6$ (horizontal dashed line) well represents the equivalent number of observing seasons if all seasons had the same number of events monitored (but with a different distribution of u_0). Hence, the planet sensitivity corrected for the number of seasons reads

$$S(\log a, \log M) \simeq \kappa\, S_{2004}(\log a, \log M)\,, \tag{5}$$

where $S_{2004}(\log a, \log M)$ is computed with the 26 events included in season 2004. We discuss in Section 3.3 the uncertainty on κ.

2.3 Host star mass distribution

As mentioned before, the host star masses are estimated via probability distributions. The mass cumulative distributions for the set of 26 events of season 2004 used to compute the detection efficiency are shown in Fig. S3 as thin black curves. The resulting mean mass cumulative distribution of this sample of events is displayed as the red bold solid curve, while the median and 68% confidence interval around the median are respectively shown as the vertical solid and

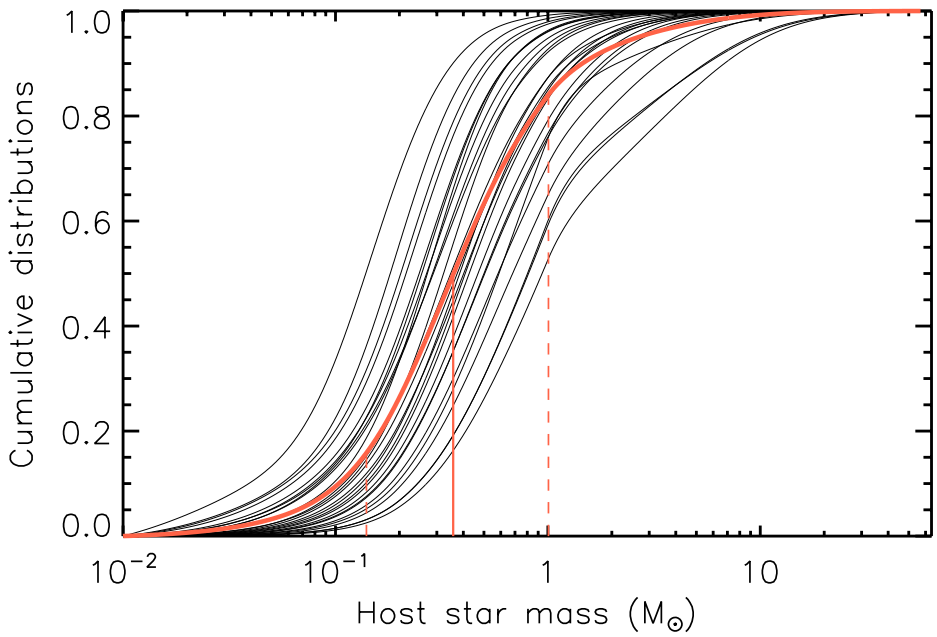

Figure S3: The thin black curves are the mass cumulative distributions of the 26 events of season 2004 used to compute the detection efficiency (or the planet sensitivity). The red bold solid curve is the resulting mean mass cumulative distribution. 68% of our probed stars lie in the mass range between the two dashed vertical lines.

dashed red lines. Hence, 68% of our probed stars lie in the mass range 0.14 to 1.0 $M_\odot$.

3 Planetary abundance

3.1 Planet detection sample

Despite ten new planets having been detected by microlensing during the 2002-2007 study interval, proper statistical treatment to arrive at the planetary mass function necessarily excludes all detections but those arising from the PLANET observing strategy as applied solely to PLANET+OGLE data. For a valid detection in that sense we demand that:

a) The event was picked up by the PLANET collaboration exclusively according to data

from OGLE-III survey-mode observations.

b) PLANET changed the observational cadence (which is then reflected in the detection efficiency as eg. a denser coverage) based only on:

   b1) anomaly alerts by real-time observational data.

   b2) the magnification of an event at given time.

c) The planetary nature of the event can be established by PLANET data and OGLE survey data alone.

Noting that OGLE high-cadence follow-up data can be treated as another PLANET-like follow-up telescope, a sample fulfilling the above guidelines can be regarded as homogeneous and legitimate. Applying these criteria we end up with the following three planet detections, which can be used in our study:

1. OGLE-2005-BLG-071Lb: OGLE high-cadence data + PLANET Canopus data collected in response to OGLE anomaly alert sufficed to establish the planetary nature of this event.

2. OGLE-2005-BLG-390Lb: PLANET detected the anomaly and PLANET+OGLE data sufficed to establish the planetary nature of this event.

3. OGLE-2007-BLG-349Lb: PLANET high-cadence data collected in response to OGLE anomaly alert. PLANET + OGLE data sufficed to to establish the planet nature of this event.

Other detections are excluded because they are either based on data arising from an observing strategy operationally distinct from that of PLANET. A planet like MOA-2007-BLG-400Lb[51] falls into this category: without the very aggressive strategy towards high-magnification events adopted by the μFUN collaboration, the planetary light curve anomaly would never have been sampled densely enough to claim a detection.

3.2 Planetary mass function

Let N be the average number of planets per lens star. Note that N needs not be an integer, thus if $0 < N < 1$, then $100 \times N$ is the percentage of the lens stars which have a planet, while if $N > 1$, it is the mean number of planetary companions per star.

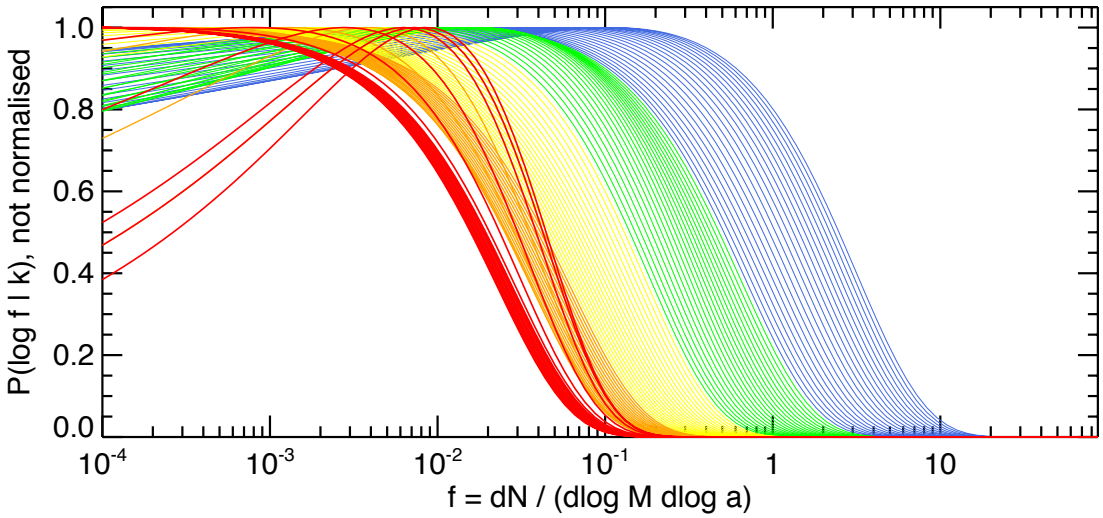

Figure S4: Posterior (unormalised) probability densities $P(\log f|k)$ computed for 100 bins equally spaced in $\log M$ dividing the mass range $5\,M_\oplus - 10\,M_\mathrm{J}$. The colours follow the rainbow order, from blue for low masses to red for higher masses.

These planets come with a range of masses M and orbit semi-major axis a, and thus with a distribution over the $(\log a, \log M)$ plane. Let $f(\log a, \log M)$ be the number of planets per star per decade of planet mass M and per decade of orbit size a,

$$f\,(\log a, \log M) \equiv \frac{\mathrm{d}^2 N}{\mathrm{d}\log a\,\mathrm{d}\log M}\,. \tag{6}$$

In our survey, the probability of detecting planets depends on the planet mass M and orbit size a. We have calculated *via* Eq. (3) the quantity $S\,(\log a, \log M)$, which is the expected number of planets that our survey can detect if all lens stars have exactly one planet of mass M and orbit size a. Then for any given planetary mass function $f(\log a, \log M)$, we can evaluate the expected number of planets that our survey detects as

$$E = \iint S\,(\log a, \log M)\, f(\log a, \log M)\,\mathrm{d}\log a\,\mathrm{d}\log M\,, \tag{7}$$

where the integration domain encloses k planet detections (k needs not be an integer). The

model then predicts a Poisson distribution

$$P(k|E) = \frac{E^k \exp(-E)}{k!}, \tag{8}$$

and with a prior distribution $P(\log f)$ for the planet abundance, the posterior distribution reads

$$P(\log f|k) = \frac{P(k|E)\,P(\log f)}{\int P(k|E)\,P(\log f)\,\mathrm{d}\log f}. \tag{9}$$

In the following, we assume an uninformative uniform prior distribution $P(\log f) = 1$. Other choices of priors slightly change the posterior distributions Eq. (9), but all are consistent within our uncertainties. This sensitivity to the assumed prior is an unavoidable consequence of the relatively limited statistics with the present sample, and a larger statistical sample would constrain this source of uncertainty. The prior distribution we choose, however, is well-suited since it assumes a uniform prior probability distribution on $\log f$, which is the quantity we aim to constrain in this analysis. Furthermore, when there is no planet detection ($k = 0$), the posterior $P(\log f|k = 0)$ distribution peaks at $f = 0$, which means only the upper limit on the planet mass function f is constrained, as would be expected.

In Figure 2, the lower panel shows the three detections (thin black lines) as probability densities $(\mathrm{d}k/\mathrm{d}\log M)_i$ that should satisfy

$$\int \left(\frac{\mathrm{d}k}{\mathrm{d}\log M}\right)_i \mathrm{d}\log M = 1 \tag{10}$$

for each individual detection i. The distributions over mass are taken from the error bars reported in the literature. The number of detections k is then computed by integrating over $\log M$ the density

$$\mathrm{d}k/\mathrm{d}\log M \equiv \sum_i (\mathrm{d}k/\mathrm{d}\log M)_i\,, \tag{11}$$

which is the red line displayed in the lower panel of Figure 2.

As an example, Fig. S4 shows the posterior probability densities $P(\log f|k)$ computed by dividing the mass range $5\,M_\oplus - 10\,M_\mathrm{J}$ into 100 bins equally spaced in $\log M$.

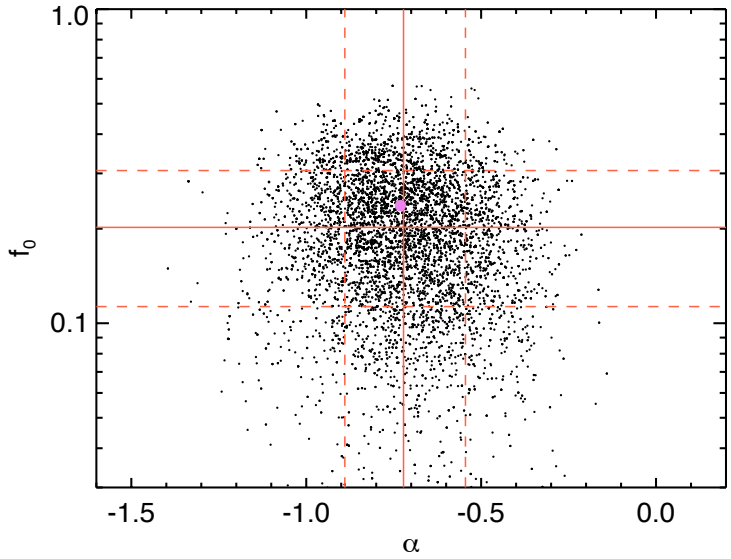

Figure S5: Posterior distributions of the two parameters α and $\log f_0$ (only a subset of the points are plotted here for display reasons) of the power-law planet mass function $f(a, M) = f_0\ (M/M_0)^{\alpha}$. The medians are marked as solid red lines, while the 68% confidence intervals around the medians are displayed as dashed red lines. The best fit is indicated by the violet dot.

3.3 Power-law planetary mass function

With the present microlensing sample, a uniform abundance model is ruled out by the data. Hence, we aim to constrain a power-law mass function of the planetary abundance of the form $f(\log a, \log M) = f_0\ (M/M_0)^{\alpha}$, that has two parameters to be determined: α, the power-law slope of the planet mass function, and f_0 the planet abundance at the fiducial planet mass M_0. In practice, M_0 is chosen as the pivot point of the fit, where α and M_0 are uncorrelated. Adding further complexity to the power-law model is not at present warranted by the data.

The power law is constrained in the range $5\,M_{\oplus} - 10\,M_{\rm J}$, for which we computed the planet sensitivity. Our results are insensitive to the adopted precise values for the upper and lower mass boundaries, by several $M_{\rm J}$ or $M_{\oplus}$, respectively. We divide the mass range into 1000 bins equally spaced in $\log M$; we note again that the result is stable when the number of bins is greater than a few hundreds.

Besides the constraint based on PLANET data that have been presented here, we also make

use in our analysis of the constraints already well-established by microlensing analyses: an estimate of $f_0 = 0.36 \pm 0.15$ derived by Ref. (43), as well an estimate of the slope $\alpha = -0.68 \pm 0.2$ published by Ref. (52). The two constraints are displayed in blue in Figure 2, respectively as the blue point and the blue lines in the upper corner of the figure. These constraints are included in the formalism by inserting Gaussian priors on α and f_0 in Eq. (9), *i.e.* multiplying the formula by

$$P(\alpha) = \exp\left(-\frac{(\alpha + 0.68)^2}{2 \times 0.2^2}\right) \tag{12}$$

$$P(f_0) = \exp\left(-\frac{(f_0' - 0.36)^2}{2 \times 0.15^2}\right) \quad \text{where } f_0' = f_0 \, (M_{\rm G10}/M_0)^{\alpha} \,, \tag{13}$$

where $M_{\rm G10} \simeq 83.2 \, M_\oplus$ is the central mass of the measurement of Ref. (43) and M_0 our pivot point.

We run a Markov Chain Monte Carlo algorithm (with Gibbs sampling) to fit for α and $\log f_0$, using the distributions $P(\log f|k)$ computed at each mass bin and the priors corresponding to previous microlensing analyses. Fig. S5 shows the posterior distribution, including 3×10^4 points to constrain the power-law planetary mass function. The medians are marked as solid red lines, while the 68% confidence intervals around the medians are displayed as dashed red lines. The best fit is indicated by the violet dot. We find

$$\alpha = -0.73 \pm 0.17 \tag{14}$$

$$f_0 = 10^{-0.62 \pm 0.22} \tag{15}$$

$$M_0 \simeq M_{\rm Sat} = 95 \, M_\oplus \,. \tag{16}$$

An additional uncertainty arises from the estimation of the equivalent number of seasons κ that was mentioned above. We find that a variation of 10% around the central value of κ (i.e. $4.2 - 5$) introduces an additional error on the parameters of the mass function that is ~ 10 times less than the uncertainty of the values quoted above.

3.4 Planetary abundance

The planetary abundance is computed from the planetary mass function following

$$N = \iint_{\mathcal{D}_a \mathcal{D}_M} f_0 \left(\frac{M}{M_0}\right)^{\alpha} \mathrm{d}\log a \, \mathrm{d}\log M \,, \tag{17}$$

in a given mass domain $\mathcal{D}_M$. The range of orbit sizes $\mathcal{D}_a$ has to stay within the range of sensitivity of microlensing observations, that can be estimated reading Figure 1. For giant planets, the sensitivity applies from 0.4 to 15 AU, with a limited sensitivity at the boundaries, while for super-Earths ($\sim 2{-}5\,M_\oplus$) the range of sensitivity is limited to ~ 2 AU. For consistency, we adopt $0.5 - 10$ AU to compare the abundance of planets for masses greater than $5\,M_\oplus$. The results for different ranges of masses are discussed in the Letter.

Table S1: List of events followed by PLANET from 2002-2007. The 26 events of the reference season 2004 for which detection efficiencies were computed are marked in boldface. The last two columns give the baseline magnitude I_0 and the Einstein radius crossing timescale t_E.

Event	R.A.	Dec	I_0	t_E
OGLE-2002-BLG-061	17:51:16.16	-30:12:31.4	17.6	185.4
OGLE-2002-BLG-103	17:50:45.43	-30:04:13.9	18.8	74.9
OGLE-2002-BLG-162	17:54:25.85	-29:54:27.5	19.9	61.8
OGLE-2002-BLG-170	17:53:55.77	-29:53:32.0	17.3	26.8
OGLE-2002-BLG-181	17:57:10.20	-29:43:41.8	17.1	69.2
OGLE-2002-BLG-217	17:56:29.86	-29:26:27.5	18.9	38.3
OGLE-2002-BLG-225	17:55:06.22	-29:24:13.0	18.9	56.5
OGLE-2002-BLG-226	17:55:21.59	-30:06:58.6	16.8	4.7
OGLE-2002-BLG-268	18:00:05.71	-29:17:10.4	20.0	10.6
OGLE-2002-BLG-280	17:49:10.73	-35:20:54.6	18.0	22.3
OGLE-2002-BLG-296	17:55:30.87	-35:25:09.1	20.3	48.1
OGLE-2002-BLG-297	17:47:33.40	-34:57:35.0	15.5	13.6
OGLE-2003-BLG-156	17:51:34.32	-29:56:09.5	21.3	92.6
OGLE-2003-BLG-158	17:54:34.01	-29:34:33.4	18.7	77.8
OGLE-2003-BLG-159	17:52:53.27	-29:54:27.6	20.6	190.1
OGLE-2003-BLG-161	17:55:09.35	-29:54:45.6	17.4	19.9
OGLE-2003-BLG-175	17:55:56.07	-30:21:39.6	17.2	59.4
OGLE-2003-BLG-177	17:47:27.50	-35:03:21.1	16.1	26.1
OGLE-2003-BLG-186	17:46:24.63	-34:53:46.0	16.4	9.0
OGLE-2003-BLG-193	17:52:55.29	-34:51:47.8	17.2	8.8
OGLE-2003-BLG-203	17:50:00.90	-34:18:13.7	13.6	40.7
OGLE-2003-BLG-204	17:46:35.76	-33:25:10.7	20.3	57.3
OGLE-2003-BLG-208	17:44:38.30	-33:31:03.9	20.5	80.9
OGLE-2003-BLG-218	17:51:56.04	-33:32:28.5	19.1	37.0
OGLE-2003-BLG-222	17:54:12.15	-32:53:17.0	19.9	45.6
OGLE-2003-BLG-223	17:58:53.25	-32:56:17.2	19.8	23.6
OGLE-2003-BLG-244	17:57:07.46	-32:59:03.2	19.1	17.6
OGLE-2003-BLG-257	18:03:00.16	-33:13:55.9	18.8	27.2
OGLE-2003-BLG-262	18:06:46.83	-32:49:12.7	15.2	12.9
OGLE-2003-BLG-269	18:05:40.00	-32:56:08.6	19.4	50.6
OGLE-2003-BLG-272	18:09:15.66	-32:50:29.3	17.5	42.7
OGLE-2003-BLG-278	18:07:39.66	-32:59:00.0	18.3	7.3
OGLE-2003-BLG-281	17:54:43.38	-32:22:49.7	17.1	17.6
OGLE-2003-BLG-285	17:57:56.26	-32:38:21.3	19.5	58.2
OGLE-2003-BLG-299	17:56:53.53	-32:31:44.0	20.2	28.7
OGLE-2003-BLG-326	18:01:24.29	-32:08:26.1	15.6	6.3
OGLE-2003-BLG-331	18:04:17.14	-32:21:18.4	15.8	8.9
OGLE-2003-BLG-334	18:12:27.36	-32:43:00.1	18.1	15.6

Table S1: continued.

Event	R.A.	Dec	I_0	t_E
OGLE-2004-BLG-191	17:52:48.06	-29:47:05.7	15.6	25.6
OGLE-2004-BLG-203	17:56:30.98	-29:25:48.5	16.2	51.3
OGLE-2004-BLG-214	17:56:10.50	-29:15:47.8	18.7	60.4
OGLE-2004-BLG-222	17:56:03.35	-29:26:56.1	17.3	30.7
OGLE-2004-BLG-234	17:53:36.29	-29:53:34.5	15.8	11.6
OGLE-2004-BLG-237	17:57:27.08	-29:13:13.0	19.0	61.0
OGLE-2004-BLG-257	17:57:28.85	-30:18:18.1	16.1	30.2
OGLE-2004-BLG-259	17:50:30.87	-36:20:19.9	18.6	40.3
OGLE-2004-BLG-274	17:49:53.66	-30:06:40.8	19.0	53.4
OGLE-2004-BLG-279	18:04:33.69	-28:54:46.3	17.7	8.4
OGLE-2004-BLG-290	17:46:51.51	-34:45:45.7	15.1	24.5
OGLE-2004-BLG-293	17:54:17.28	-33:30:24.0	17.9	13.5
OGLE-2004-BLG-298	17:57:33.99	-33:25:18.4	18.3	16.0
OGLE-2004-BLG-299	17:56:21.88	-33:08:41.9	20.9	25.0
OGLE-2004-BLG-305	17:53:54.50	-33:02:55.2	19.8	18.6
OGLE-2004-BLG-315	17:57:23.69	-33:06:10.4	16.4	7.6
OGLE-2004-BLG-319	17:53:47.89	-32:35:54.5	16.7	24.1
OGLE-2004-BLG-335	17:54:05.60	-31:45:54.4	19.1	13.5
OGLE-2004-BLG-342	17:52:07.38	-31:56:20.8	16.3	63.0
OGLE-2004-BLG-351	17:57:46.85	-31:42:03.5	19.7	18.9
OGLE-2004-BLG-364	18:01:46.61	-31:33:21.5	15.6	37.7
OGLE-2004-BLG-382	18:00:00.73	-31:56:35.9	19.6	13.2
OGLE-2004-BLG-384	17:56:36.03	-30:59:57.5	15.9	44.0
OGLE-2004-BLG-390	17:58:34.71	-29:58:34.3	17.8	28.9
OGLE-2004-BLG-393	17:52:06.69	-29:55:15.9	19.9	58.5
OGLE-2004-BLG-398	17:58:46.00	-29:07:43.3	18.5	45.2
OGLE-2004-BLG-407	18:10:34.35	-28:12:37.9	17.2	24.0
OGLE-2004-BLG-409	18:09:28.02	-28:01:25.1	19.4	8.6
OGLE-2004-BLG-416	17:45:21.41	-33:31:15.8	21.4	45.7
OGLE-2004-BLG-421	17:45:33.99	-24:26:43.1	18.6	14.0
OGLE-2004-BLG-434	17:51:25.77	-29:53:50.2	19.3	20.8
OGLE-2004-BLG-435	17:55:38.49	-32:43:45.6	20.2	28.4
OGLE-2004-BLG-441	17:57:58.34	-31:12:46.0	16.7	5.4
OGLE-2004-BLG-442	17:50:30.06	-30:30:43.1	19.3	58.6
OGLE-2004-BLG-446	17:58:22.69	-30:46:37.2	19.1	18.0
OGLE-2004-BLG-448	18:02:00.11	-30:39:03.0	18.9	10.1
OGLE-2004-BLG-458	18:00:43.48	-29:53:14.8	19.3	34.4
OGLE-2004-BLG-462	18:01:14.89	-29:47:42.4	20.9	48.7
OGLE-2004-BLG-479	17:50:59.02	-29:40:33.8	20.8	33.8
OGLE-2004-BLG-487	17:47:13.41	-36:24:04.7	18.6	12.7
OGLE-2004-BLG-496	17:50:26.94	-35:47:39.2	18.4	26.7
OGLE-2004-BLG-515	18:06:17.76	-29:16:53.2	16.4	21.6
OGLE-2004-BLG-528	17:56:40.45	-28:05:27.9	16.1	9.2

Table S1: continued.

Event	R.A.	Dec	I_0	t_E
OGLE-2005-BLG-099	17:54:55.01	-30:01:28.4	14.5	53.2
OGLE-2005-BLG-120	17:57:46.56	-29:05:30.8	16.8	26.8
OGLE-2005-BLG-158	17:57:40.04	-28:50:40.7	15.4	19.7
OGLE-2005-BLG-191	17:57:33.15	-28:43:06.6	18.0	39.4
OGLE-2005-BLG-201	17:52:32.36	-32:32:54.7	18.4	15.6
OGLE-2005-BLG-215	17:55:53.10	-31:42:10.8	18.8	68.2
OGLE-2005-BLG-216	17:54:20.38	-32:00:13.7	19.3	30.7
OGLE-2005-BLG-222	17:55:55.60	-31:17:33.3	17.3	17.1
OGLE-2005-BLG-234	17:55:13.56	-31:03:43.7	19.9	36.4
OGLE-2005-BLG-241	17:54:09.27	-31:15:38.8	18.7	20.9
OGLE-2005-BLG-245	17:49:46.87	-30:55:09.5	16.8	53.6
OGLE-2005-BLG-259	17:57:48.61	-30:27:21.3	14.1	39.3
OGLE-2005-BLG-265	18:01:24.25	-30:45:42.2	16.0	18.4
OGLE-2005-BLG-277	17:52:08.51	-30:09:18.2	21.0	274.9
OGLE-2005-BLG-288	18:04:29.96	-30:10:33.1	15.4	15.0
OGLE-2005-BLG-292	18:03:40.93	-29:43:09.8	16.8	10.7
OGLE-2005-BLG-304	18:07:41.44	-29:42:38.6	15.1	31.3
OGLE-2005-BLG-312	18:09:19.61	-29:41:39.5	19.6	25.2
OGLE-2005-BLG-324	17:56:58.03	-28:50:40.2	18.8	42.2
OGLE-2005-BLG-333	18:00:10.24	-29:04:48.8	18.9	9.8
OGLE-2005-BLG-338	17:58:38.62	-28:54:06.7	18.3	15.1
OGLE-2005-BLG-349	18:02:36.31	-28:48:02.6	19.7	34.4
OGLE-2005-BLG-352	18:02:30.23	-28:41:45.2	20.1	18.9
OGLE-2005-BLG-356	18:03:54.57	-28:45:15.7	18.5	55.6
OGLE-2005-BLG-360	18:00:36.63	-28:27:42.5	19.6	27.5
OGLE-2005-BLG-368	18:00:24.45	-27:50:19.1	20.1	54.1
OGLE-2005-BLG-370	18:00:11.74	-26:52:51.8	15.5	28.8
OGLE-2005-BLG-393	17:59:10.13	-27:23:15.8	20.8	28.8
OGLE-2005-BLG-404	18:03:03.14	-27:13:28.6	19.7	9.9
OGLE-2005-BLG-407	18:06:25.17	-27:21:43.8	18.1	26.7
OGLE-2005-BLG-420	18:07:29.83	-26:34:42.4	19.1	29.4
OGLE-2005-BLG-433	18:12:49.67	-26:47:06.5	17.8	29.8
OGLE-2005-BLG-435	18:11:29.35	-25:38:24.4	19.1	22.1
OGLE-2005-BLG-436	17:54:57.92	-32:21:21.2	16.9	12.9
OGLE-2005-BLG-440	17:56:05.07	-31:52:50.6	19.8	35.6
OGLE-2005-BLG-454	18:02:26.09	-29:15:52.5	18.9	76.6
OGLE-2005-BLG-455	18:05:42.86	-28:55:16.3	19.6	7.6
OGLE-2005-BLG-465	18:05:55.13	-28:51:18.7	20.6	24.8
OGLE-2005-BLG-495	18:02:48.61	-28:06:42.8	19.2	18.1
OGLE-2005-BLG-497	18:04:06.39	-28:16:50.1	15.2	11.7
OGLE-2005-BLG-501	17:59:18.86	-27:36:10.0	17.6	16.4

Table S1: continued.

Event	R.A.	Dec	I_0	t_E
OGLE-2006-BLG-094	17:51:43.96	-29:42:19.5	17.0	38.3
OGLE-2006-BLG-123	17:54:40.83	-29:46:08.9	17.0	18.5
OGLE-2006-BLG-168	17:59:42.72	-29:22:30.5	19.1	84.2
OGLE-2006-BLG-178	18:02:43.39	-29:19:56.0	16.4	11.4
OGLE-2006-BLG-180	17:50:04.55	-34:58:15.7	16.7	18.5
OGLE-2006-BLG-181	17:58:07.47	-30:50:12.8	20.5	55.7
OGLE-2006-BLG-195	18:01:35.61	-29:46:26.7	19.0	8.3
OGLE-2006-BLG-208	17:51:52.13	-29:35:33.3	20.5	18.0
OGLE-2006-BLG-225	17:54:07.47	-29:08:13.5	19.0	11.1
OGLE-2006-BLG-236	17:58:32.41	-28:34:02.3	17.9	21.6
OGLE-2006-BLG-237	17:59:57.13	-28:20:26.1	19.7	43.4
OGLE-2006-BLG-247	18:08:15.28	-28:19:21.6	15.9	8.2
OGLE-2006-BLG-253	17:59:09.49	-27:30:12.4	18.5	27.6
OGLE-2006-BLG-259	18:05:46.20	-27:31:53.6	16.3	12.1
OGLE-2006-BLG-265	18:05:51.82	-27:52:23.4	19.4	28.6
OGLE-2006-BLG-280	18:01:04.17	-27:11:12.8	19.9	34.6
OGLE-2006-BLG-297	17:51:05.25	-29:52:11.3	18.6	18.7
OGLE-2006-BLG-306	17:52:15.82	-29:42:16.2	17.0	37.5
OGLE-2006-BLG-326	17:47:26.99	-33:58:08.2	19.7	17.2
OGLE-2006-BLG-336	17:53:15.15	-33:17:23.6	16.1	17.9
OGLE-2006-BLG-341	17:51:30.76	-32:42:26.6	20.2	17.8
OGLE-2006-BLG-347	17:55:05.15	-32:28:51.3	19.2	31.7
OGLE-2006-BLG-349	18:05:16.70	-26:45:03.4	15.5	17.3
OGLE-2006-BLG-355	17:56:32.46	-30:12:43.4	19.9	29.2
OGLE-2006-BLG-361	18:00:03.01	-29:31:14.7	19.1	53.9
OGLE-2006-BLG-371	17:53:08.22	-31:12:17.8	19.7	8.7
OGLE-2006-BLG-374	17:59:27.37	-29:08:12.8	17.2	31.6
OGLE-2006-BLG-377	17:55:55.71	-29:29:19.4	20.1	108.7
OGLE-2006-BLG-381	18:08:46.06	-28:12:34.9	19.7	16.1
OGLE-2006-BLG-396	17:51:39.39	-32:10:51.9	18.7	19.5
OGLE-2006-BLG-403	17:53:57.53	-30:53:17.5	19.2	35.1
OGLE-2006-BLG-416	17:58:43.51	-30:25:00.6	19.6	25.8
OGLE-2006-BLG-417	17:57:05.53	-29:03:43.9	18.0	15.4
OGLE-2006-BLG-419	17:59:13.75	-28:55:30.0	20.3	45.8
OGLE-2006-BLG-440	18:08:46.38	-28:01:46.2	20.6	43.4
OGLE-2006-BLG-448	17:51:02.87	-29:39:41.1	19.8	31.8
OGLE-2006-BLG-460	17:51:49.84	-29:27:47.9	22.1	131.5
OGLE-2006-BLG-476	17:53:41.06	-29:27:02.6	19.9	11.9

Table S1: continued.

Event	R.A.	Dec	I_0	t_E
OGLE-2007-BLG-043	17:53:47.21	-29:44:23.7	18.6	63.8
OGLE-2007-BLG-147	17:54:06.64	-29:37:55.4	19.1	51.9
OGLE-2007-BLG-155	17:59:43.42	-29:40:29.9	16.5	21.6
OGLE-2007-BLG-161	17:58:39.75	-29:16:24.6	16.1	46.8
OGLE-2007-BLG-218	18:02:04.61	-29:20:39.5	17.5	64.8
OGLE-2007-BLG-220	17:42:42.80	-34:26:27.2	21.8	72.1
OGLE-2007-BLG-239	17:45:22.79	-34:02:40.3	19.1	52.6
OGLE-2007-BLG-251	17:49:21.37	-33:38:24.2	19.2	3.4
OGLE-2007-BLG-252	17:52:25.55	-32:42:59.8	20.1	42.7
OGLE-2007-BLG-255	17:53:36.17	-31:17:05.0	17.5	46.1
OGLE-2007-BLG-262	17:52:37.27	-31:11:35.7	20.9	12.4
OGLE-2007-BLG-268	17:56:15.07	-31:11:14.7	17.2	18.5
OGLE-2007-BLG-284	17:51:24.16	-30:37:32.3	16.4	24.0
OGLE-2007-BLG-287	17:55:48.22	-30:45:48.3	15.1	20.5
OGLE-2007-BLG-294	18:02:32.64	-30:49:13.6	19.0	38.5
OGLE-2007-BLG-295	17:50:27.88	-29:40:40.5	20.2	14.2
OGLE-2007-BLG-299	17:52:55.92	-29:05:43.5	16.5	31.6
OGLE-2007-BLG-302	17:53:24.43	-29:26:30.8	16.3	16.3
OGLE-2007-BLG-308	18:05:22.84	-28:38:57.8	17.7	12.2
OGLE-2007-BLG-319	17:58:54.69	-28:31:12.8	19.5	11.8
OGLE-2007-BLG-333	17:59:59.20	-27:58:00.4	17.0	11.3
OGLE-2007-BLG-344	18:01:14.54	-27:40:02.7	19.9	39.8
OGLE-2007-BLG-353	17:56:21.84	-29:25:12.1	16.8	27.6
OGLE-2007-BLG-354	17:49:21.40	-33:38:24.8	19.9	31.8
OGLE-2007-BLG-369	17:54:56.26	-33:07:43.8	20.7	62.5
OGLE-2007-BLG-370	17:53:59.04	-32:09:48.7	20.2	10.1
OGLE-2007-BLG-382	17:56:05.85	-31:56:48.8	18.3	6.9
OGLE-2007-BLG-394	17:55:11.27	-31:57:06.3	16.0	12.1
OGLE-2007-BLG-430	17:58:00.44	-31:01:40.5	19.6	28.8
OGLE-2007-BLG-451	17:52:48.33	-30:42:24.3	19.2	39.7
OGLE-2007-BLG-457	18:05:34.71	-30:44:19.5	18.9	18.4
OGLE-2007-BLG-464	18:10:25.85	-29:39:53.8	15.3	20.0
OGLE-2007-BLG-467	17:59:46.49	-28:43:03.3	18.5	30.2
OGLE-2007-BLG-471	18:03:43.23	-29:09:42.2	19.9	25.1
OGLE-2007-BLG-485	17:58:24.86	-27:29:39.8	21.0	10.3
OGLE-2007-BLG-567	18:04:36.09	-27:25:42.1	17.3	9.3

References

[31] Mayor, M. & Queloz, D. A Jupiter-Mass Companion to a Solar-Type Star. *Nature* **378**, 355 (1995).

[32] Udalski, A. The Optical Gravitational Lensing Experiment. Real Time Data Analysis Systems in the OGLE-III Survey. *Acta Astron.* **53**, 291–305 (2003).

[33] Bond, I. A. *et al.* Real-time difference imaging analysis of MOA Galactic bulge observations during 2000. *Mon. Not. R. Astron. Soc.* **327**, 868–880 (2001).

[34] Albrow, M. *et al.* The 1995 Pilot Campaign of PLANET: Searching for Microlensing Anomalies through Precise, Rapid, Round-the-Clock Monitoring. *Astrophys. J.* **509**, 687–702 (1998).

[35] Gould, A. & Loeb, A. Discovering planetary systems through gravitational microlenses. *Astrophys. J.* **396**, 104–114 (1992).

[36] Gaudi, B. S. *et al.* Microlensing constraints on the frequency of jupiter-mass companions: Analysis of 5 years of planet photometry. *Astrophys. J.* **566**, 463–499. (2002).

[37] Snodgrass, C., Horne, K., & Tsapras, Y. The abundance of Galactic planets from OGLE-III 2002 microlensing data. *Mon. Not. R. Astron. Soc.* **351**, 967–975 (2004).

[38] Gaudi, B. S. & Sackett, P. D. Detection Efficiencies of Microlensing Data Sets to Stellar and Planetary Companions. *Astrophys. J.* **528**, 56–73 (2000).

[39] Schechter, P. L., Mateo, M., & Saha, A. DOPHOT, a CCD photometry program: Description and tests. *Publ. Astron. Soc. Pacif.* **105**, 1342–1353 (1993).

[40] Einstein, A. Lens-Like Action of a Star by the Deviation of Light in the Gravitational Field. *Science* **84**, 506–507 (1936).

[41] Paczynski, B. Gravitational microlensing by the galactic halo. *Astrophys. J.* **304**, 1–5 (1986).

[42] Mao, S. & Paczynski, B. Gravitational microlensing by double stars and planetary systems. *Astrophys. J.* **374**, L37–L40 (1991).

[43] Gould, A. *et al.* Frequency of Solar-like Systems and of Ice and Gas Giants Beyond the Snow Line from High-magnification Microlensing Events in 2005-2008. *Astrophys. J.* **720**, 1073–1089 (2010).

[44] Cassan, A. PhD thesis, Searching for extra-solar planets and probing the atmosphere of Bulge giant stars through gravitational microlensing, Institut d'Astrophysique de Paris / Université Pierre et Marie Curie, (2005).

[45] Kubas, D. PhD thesis, Applications of Galactic Microlensing, University of Potsdam, (2005).

[46] Cassan, A. An alternative parameterisation for binary-lens caustic-crossing events. *Astron. Astrophys.* **491**, 587–595 (2008).

[47] Cassan, A., Horne, K., Kains, N., Tsapras, Y., & Browne, P. Bayesian analysis of caustic-crossing microlensing events. *Astron. Astrophys.* **515**, A52 (2010).

[48] Wambsganss, J. Discovering Galactic planets by gravitational microlensing: magnification patterns and light curves. *Mon. Not. R. Astron. Soc.* **284**, 172–188 (1997).

[49] Dominik, M. Stochastic distributions of lens and source properties for observed galactic microlensing events. *Mon. Not. R. Astron. Soc.* **367**, 669–692 (2006).

[50] Kubas, D. *et al.* Limits on additional planetary companions to OGLE 2005-BLG-390L. *Astron. Astrophys.* **483**, 317–324 (2008).

[51] Dong, S. *et al.* Microlensing Event MOA-2007-BLG-400: Exhuming the Buried Signature of a Cool, Jovian-Mass Planet. *Astrophys. J.* **698**, 1826–1837 (2009).

[52] Sumi, T. *et al.* A Cold Neptune-Mass Planet OGLE-2007-BLG-368Lb: Cold Neptunes Are Common. *Astrophys. J.* **710**, 1641–1653 (2010).